Biochemical and Biophysical Research Communications 438 (2013) 594–599

Contents lists available at ScienceDirect

Biochemical and Biophysical Research Communications

journal homepage: www.elsevier.com/locate/ybbrc

Three-dimensional modulation of cortical plasticity during pseudopodial protrusion of mouse leukocytes

Hiromi Miyoshi [a], Ken-ichi Tsubota [b,*], Takamasa Hoyano [b], Taiji Adachi [c], Hao Liu [b,d]

[a] Ultrahigh Precision Optics Technology Team, RIKEN Center for Advanced Photonics, Saitama, Japan
[b] Graduate School of Engineering, Chiba University, Chiba, Japan
[c] Department of Biomechanics, Institute for Frontier Medical Sciences, Kyoto University, Kyoto, Japan
[d] Shanghai Jiao Tong University and Chiba University International Cooperative Research Centre (SJTU-CU ICRC), Shanghai Jiao Tong University, Shanghai, China

ARTICLE INFO

Article history:
Received 30 July 2013
Available online 11 August 2013

Keywords:
Leukocyte
Cell migration
Amoeboid type movement
Pseudopodial protrusion
Cortical flow

ABSTRACT

Leukocytes can rapidly migrate virtually within any substrate found in the body at speeds up to 100 times faster than mesenchymal cells that remain firmly attached to a substrate even when migrating. To understand the flexible migration strategy utilized by leukocytes, we experimentally investigated the three-dimensional modulation of cortical plasticity during the formation of pseudopodial protrusions by mouse leukocytes isolated from blood. The surfaces of viable leukocytes were discretely labeled with fluorescent beads that were covalently conjugated with concanavalin A receptors. The movements of these fluorescent beads were different at the rear, central, and front surfaces. The beads initially present on the rear and central dorsal surfaces of the cell body flowed linearly toward the rear peripheral surface concomitant with a significant collapse of the cell body in the dorsal–ventral direction. In contrast, those beads initially on the front surface moved into a newly formed pseudopodium and exhibited rapid, random movements within this pseudopodium. Bead movements at the front surface were hypothesized to have resulted from rupture of the actin cytoskeleton and detachment of the plasma membrane from the actin cytoskeletal cortex, which allowed leukocytes to migrate while being minimally constrained by a substrate.

1. Introduction

Migrating cells *in vivo* exhibit several basic processes, including cytoplasmic protrusion at their leading edge, adhesion to the extracellular matrix (ECM), and generating force against this adhesion to move the cell body forward. Although the same basic processes are involved, different cell types exhibit different modes of migration related to their specific functions. Inflammatory cells utilize rapid, flexible migration strategies to mount an effective immune response [1]. In particular, leukocytes can move virtually within any substrate found in the body at speeds up to 100 times faster than mesenchymal cells that remain firmly attached to the ECM even when migrating [2].

Because the physical characteristics of cytoplasmic protrusion at the leading edge and cell body translocation are major determinants of the mode of cell migration [3], studies from the mechanical viewpoint are essential for understanding the rapid, flexible migration strategy utilized by leukocytes. Leukocyte migration is characterized by pseudopodial amoeboid type movement [2]. Cells that migrate by amoeboid type movement do not have bundled actin stress fibers or focal adhesions. This is in contrast to mesenchymal cell movement that is typically exhibited by fibroblasts with developed stress fibers that contribute to retracting the cell body and focal adhesions that firmly link actin stress fibers and the ECM. During amoeboid type movement, a contractile actomyosin cortex under the lipid membrane and loose contacts between a cell and a substrate are responsible for force generation [4]. These differences in physical characteristics determine the migration strategy of whether a cell can migrate only on a defined substrate or flexibly interact and migrate on any substrate, as leukocytes do [5]. Thus, determining cell cortex mechanics is essential for understanding the rapid, flexible migration strategies utilized by leukocytes [1].

Although significant progress has been made in elucidating the molecular mechanisms that underlie cell migration [6], quantitative characterizations of the associated cellular mechanical properties remain largely incomplete, particularly for amoeboid type migration. The physical behaviors of lamellar and lamellipodial protrusions that are typical of mesenchymal cell movement and keratocyte-like movement are well understood based on subcellular observations of the dynamics of the actin cytoskeleton using fluorescent speckle microscopy [7–10]. Actin cytoskeletal dynamics in thin lamellipodia and lamellae can be investigated by tracking markers on them based on time course images in only one focal plane [11]. In contrast, cell cortex dynamics during amoe-

* Corresponding author.
E-mail address: tsubota@faculty.chiba-u.jp (K.-i. Tsubota).

0006-291X/$ - see front matter © 2013 Elsevier Inc. All rights reserved.
http://dx.doi.org/10.1016/j.bbrc.2013.08.010

boid type migration are three-dimensional (3D). Technical difficulties with 3D tracking of markers have been a drawback for clarifying cell cortex mechanics.

The aim of our study was to characterize those cell cortex physical behaviors that underlie rapid, flexible migration strategies utilized by leukocytes during their amoeboid movement. To investigate cortex physical behaviors three-dimensionally, we used carboxylate-modified fluorescent latex beads to discretely label the cell surface. These carboxylate-modified beads were covalently conjugated to a known cell surface receptor, concanavalin A (Con A) [12,13]. The movements of many kinds of surface receptors involving Con A have been shown to reflect the interactions between the cell membrane and the underlying cytoskeleton [14]. Furthermore, when Con A is present on the membrane of a cell with an actin rich cortex, the movement of Con A is tightly coupled to the motility of the actin cortex [12]. Using this method with mouse leukocytes isolated from blood, we successfully determined the 3D modulation of cortical plasticity during pseudopodial protrusion at subcellular resolution.

2. Materials and methods

2.1. Cell isolation

A drop of fresh mouse blood was obtained from a tail puncture and mixed with Ringer's acetate solution (Physio140 Injection, Otsuka Pharmaceutical). Leucocytes were then isolated by density gradient centrifugation at 500×*g* for 15 min using Lymphosepar II (*d* = 1.090; Immuno-Biology Laboratories). The fraction containing leucocytes was diluted with modified Ringer's acetate solution supplemented with 1.48×10^{-3} mol/l $MgCl_2 \cdot 6H_2O$ and 0.2% fetal bovine serum. The cell suspension was then placed on a glass bottom dish (MatTek) that had been precoated with fibronectin (5 μg/cm^2) and the cells were allowed to settle and adhere to the bottom glass.

2.2. Labeling viable leukocyte surfaces with fluorescent beads

Yellow–green carboxylate-modified beads (diameter = 0.1 μm, 2% suspension in water; Molecular Probes, Inc., Eugene, OR) were diluted to 1:1000 with modified Ringer's acetate solution. Cells that had adhered to the glass bottom dish were incubated with this solution for 10 min, after which the cells were washed several times with modified Ringer's acetate solution.

2.3. Microscopy

To induce chemotaxis, 2 nM formyl-Methionyl-Leucyl-Phenylalanine (fMLP) was filled in a glass micropipette (tip diameter = 3 μm), and then applied by pressure ejection from the micropipette placed at 100 μm from a cell.

To detect a cell's outline and whole cell cortex dynamics, a time series of image sets was acquired consisting of a differential interference contrast (DIC) image of the cell (Fig. 1A) in one focal plane and fluorescent bead images (Fig. 1B) in different focal planes (0.5 μm intervals) using a confocal microscope (FV1000D, Olympus). For some experiments, a time series of image data sets was acquired with an inverted microscope with a 100× 1.4NA Plan objective lens (Olympus) and an iXonEM EMCCD camera (Andor Technology) controlled with live cell imaging software (Andor iQ, Andor Technology). Image sets were acquired every 20 s for 6 different leukocytes.

To acquire images focusing on the rapid beads movements on a leukocyte pseudopodium, bead images in a single focal plane were acquired by wide-field fluorescent microscopy every second using an inverted microscope with a 100× 1.4NA Plan objective lens (Olympus) and an iXonEM EMCCD camera (Andor Technology) controlled with live cell imaging software (Andor iQ, Andor Technology). Image acquisition was performed for 3 different leukocytes.

2.4. Image analysis for bead movements

Using the method illustrated in Fig. 1C, the 3D position (x_i, y_i, z_i) of a fluorescent bead was manually acquired in a Cartesian coordinate system for the *i*th image data set at some time, t_i, based on the criteria that the center of the fluorescent signal was the *xy*-position of the bead and the position of the focal plane with maximum bead fluorescent intensity corresponded to its *z*-position.

To characterize the dynamics at the rear, center, and front surfaces of a cell, as illustrated in Fig. 1D, we defined a relative coordinate system, (x', y', z), which was fixed to the movement of the cell's center of mass. Then, the relative velocity, $v'_i = \left(v'_{x'i}, v'_{y'i}, v'_{zi}\right)$, with reference to the cell's center of mass for a time interval, $\Delta t = t_{i+5} - t_i$, was calculated. To quantitatively define the rear, center, and front surfaces of a cell, the x'-position was normalized as x'^* by dividing the x'-position with reference to the cell diameter, $R = 2\sqrt{\bar{S}/\pi}$, where $\bar{S}$ was the mean $x'y'$-projected area of the cell to be analyzed. The rear, central, and front surfaces were those regions with $-1 < x'^* \leq -0.5$, $-0.5 < x'^* \leq 0$, and $0 < x'^* \leq 0.5$, respectively.

Rapid, random movements of the beads on the surface of a newly forming pseudopodium were characterized by a diffusion coefficient. The diffusion coefficient was estimated based on the mean-square displacement [14]:

$$\mathrm{MSD}(\Delta t_n) = \frac{1}{N-1-n}\sum_{j=1}^{N-1-n}\left[(x_{j+n}-x_j)^2 + (y_{j+n}-y_j)^2\right],$$

where $\Delta t_n = t_{i+n} - t_i$, N was the total number of image sets in a time sequence, n and j were positive integers, and n was the time increment.

3. Results

Fluorescent carboxylate-modified beads on the surfaces of 6 different leukocytes during pseudopodial protrusion were tracked. A representative time sequence of bead movements during pseudopodial protrusion is shown in Fig. 2. As seen in the DIC image in Fig. 2A (left column), at t = 4.4 s, the leukocyte exhibited a round shape. Subsequently, the cell began to extend two pseudopodia toward the bottom left and right of the figure at t = 97.9 s. Then, the bottom left pseudopodium retracted toward the main cell body, whereas the bottom right pseudopodium remained extended from t = 97.9 s to 359.7 s. During pseudopodial protrusion, the integrated distance that the cell travelled was 17.3 μm for 374 s; the average speed was 17.3 μm/374 s = 0.05 μm/s. The mean speed of 6 different leukocytes was 0.04 ± 0.01 μm/s.

The movements of the fluorescent beads were observed with a confocal microscope (middle and right columns in Fig. 2A). The spatial and temporal intervals of the confocal optical slice images were 0.5 μm and 1.1 s, respectively, and 17 optical slice images were required to three-dimensionally observe all the beads on a whole single cell. This image acquisition condition allowed us to three-dimensionally track bead movements on a whole single cell cortex. For the leukocyte in Fig. 2, the positions of 28 beads could be determined. The positions of the beads projected on the *xy*-plane and *xz*-plane are shown in Fig. 2B and C, respectively. The movements of 8 randomly selected beads were tracked and are shown by colored symbols in Fig. 2B and C.

A bead that was on the rear peripheral surface of the cell body at t = 0 (bead No. 1 in Fig. 2B and C) remained on the rear periph-

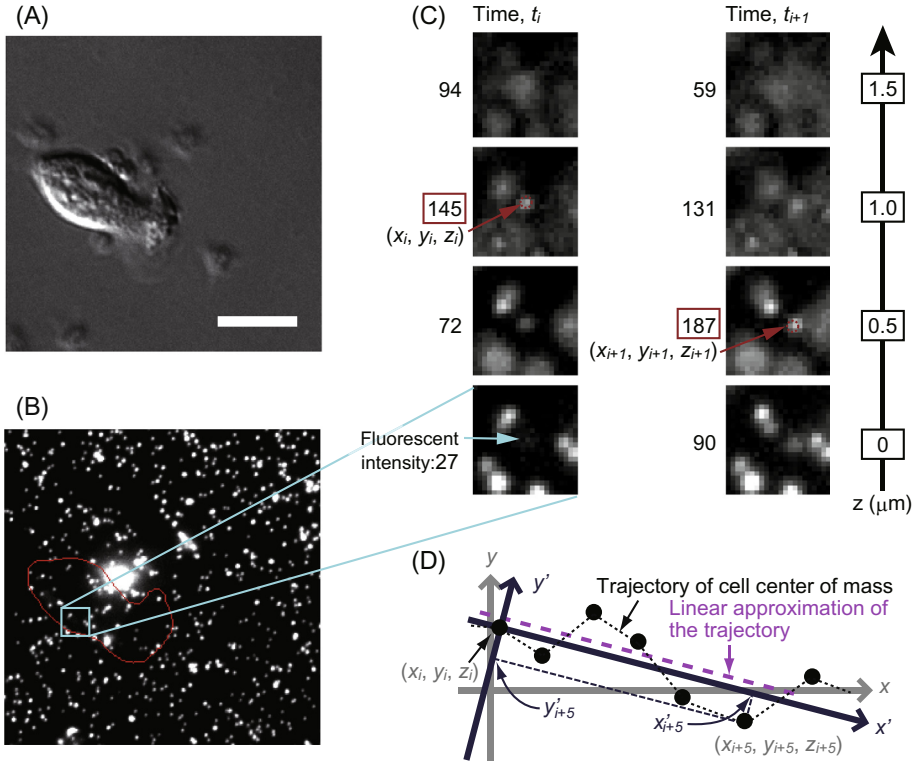

Fig. 1. Scheme for quantitatively analyzing fluorescent bead movements on a leukocyte surface. (A) DIC image of a leukocyte. Scale bar = 10 μm. (B) Fluorescent bead image in the focal plane of the bottom glass (z = 0 μm). The red line indicates the cell outline curve extracted from the DIC image in (A). (C) The position of a fluorescent bead at each time point was determined from the fluorescent images of the bead acquired in different focal planes. First, the image showing the maximum fluorescence intensity of the bead is identified and the position of the focal plane is defined as the z-position of the bead (z_i = 1.0 μm at t_i, and z_{i+1} = 0.5 μm at t_{i+1}). The center of maximum fluorescence is defined as the xy-position of the bead. (D) Definitions of the x'-axis and the y'-axis in a relative coordinate system, (x', y', z). The x'-axis is parallel to the linear approximation for the trajectory of the cell center of mass indicated by the magenta dashed line. The positive direction of the x'-axis corresponds to the movement direction of the cell center of mass. The origin in this coordinate system at time t_i corresponds to the position of the cell center of mass at time t_i. (For interpretation of the references to color in this figure legend, the reader is referred to the web version of this article.)

eral surface throughout the observation period. The same tendency for the beads that were on rear peripheral surfaces was also observed for all 6 leukocytes investigated.

Beads that were on the central dorsal surface of the cell body at t = 0 (beads No. 3–7 in Fig. 2B and C) displayed significant changes in their z-positions from larger to smaller values, whereas there was little change in their xy-positions. These displacements were assumed to be coupled to the displacement of the dorsal cortex of the cell body toward the ventral direction. The same tendency for the displacement of the dorsal cortex toward the ventral direction was typical during the extension of one broad, large pseudopodium, as observed for 5 leukocytes. In one case when a leukocyte exhibited less pseudopodium protrusion, bead displacements in the z-direction were small.

Those beads that were on the front peripheral surface of the cell body at t = 0 (beads Nos. 2 and 8 in Fig. 2B and C) moved toward the surface of a newly forming pseudopodium. An analysis of 5 leukocytes demonstrated that 70% beads that were on the front periphery of the cortex before pseudopodial protrusion moved onto the surface of a newly forming pseudopodium, while the remaining 30% beads remained on the cortex of the main cell body.

After moving onto the surface of a newly forming pseudopodium, as observed for bead Nos. 2 and 8 in Fig. 2B and C, the speed of the bead movements increased. In addition, their direction of movement was not the same. Sometimes it was the same as the pseudopodial protrusion direction (bead No. 2, t = 97.9–191.4 s; bead No. 8, t = 191.4–284.9 s), opposite this direction (bead No. 8, t = 284.9–359.7 s) or at other times it was random (bead No. 2, t = 191.4–359.7 s). An MSD analysis ($\Delta t_n \leq 100$ s) of the bead movements on newly forming pseudopodia for 3 different leukocytes showed that >90% of the movement trajectories were due to simple Brownian movement. The diffusion coefficient for the beads was of the order 1×10^{-10} cm^2/s.

The results for bead tracking shown in Fig. 2 clearly indicated the heterogeneity of the surface dynamics within a single leukocyte during pseudopodial protrusion. We statistically characterized the heterogeneity of the bead movements on the leukocyte surfaces at subcellular spatial resolutions. To extract the surface dynamics by removing the effects of a cell's translocation, velocity, $v' = \left(v'_{x\prime}, v'_{y\prime}, v'_z\right)$, relative to a cell's center of mass was estimated for 8 randomly selected beads. For these velocity estimations, a time interval of 100 s was used. Velocity, v', was estimated for each of 6 different leukocytes. To visualize the heterogeneity of surface dynamics depending on the region of a cell's surface, the components of the relative velocity, $v'_{x\prime}$, $v'_{y\prime}$, and v'_z, were plotted against the position x' (Fig. 3A). The mean values, $\langle v'_{x\prime}\rangle$, $\langle v'_{y\prime}\rangle$ and $\langle v'_z\rangle$ of $v'_{x\prime}$, $v'_{y\prime}$, and v'_z, respectively, for the rear $(-1 < x'^* \leq -0.5)$, central $(-0.5 < x'^* \leq 0)$, and front $(0 < x'^* \leq 0.5)$ cell surfaces were estimated and are shown in Fig. 3B. In addition, the mean values, $\langle \left| v'_{x\prime y\prime z} \right| \rangle$, of $\left| v'_{x\prime y\prime z} \right|$ for the rear $(-1 < x'^* \leq -0.5)$, central $(-0.5 < x'^* \leq 0)$, and front $(0 < x'^* \leq 0.5)$ cell surfaces were estimated and are shown in Fig. 3C.

As shown in Fig. 3A, the relative velocities, $v'_{x\prime}$, were widely distributed and had a tendency to be high in the front region than in the rear and central regions. In Fig. 3B, the values of $\langle v'_{x\prime}\rangle$ were negative, except for the front peripheral surface $(0.25 < x'^* \leq 0.5)$, which indicated that the bead movements in the x' direction on the rear and central surfaces were opposite to that of cell migration

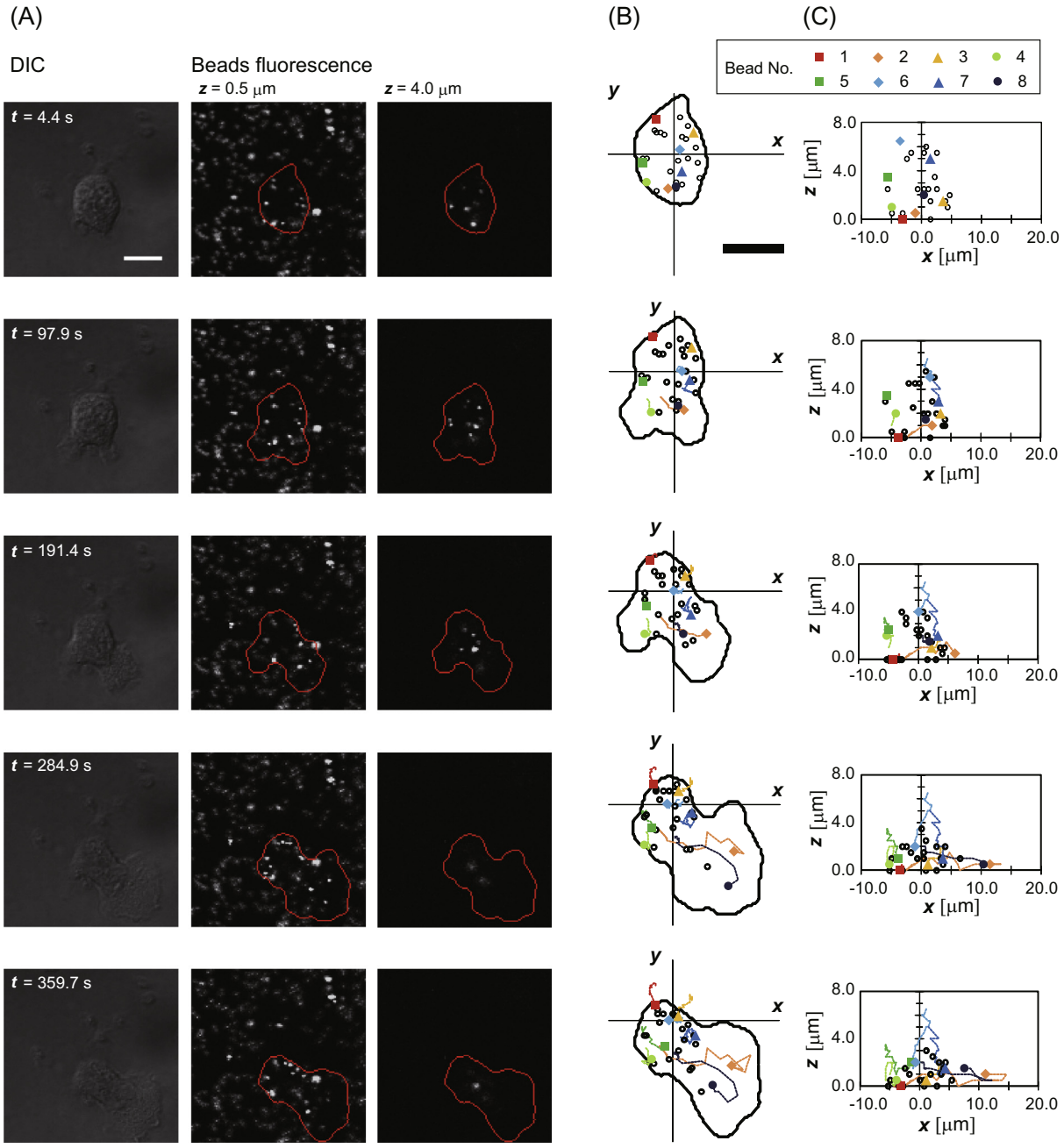

Fig. 2. Bead movements on the surface of a leukocyte during pseudopodial protrusion. (A) Time series of DIC images of a cell (left column), bead fluorescent images at $z = 0.5$ μm (middle column), and at $z = 4.0$ μm (right column). The red cell outline curve extracted from the DIC image is merged on the fluorescent image (middle and right columns). (B, C) 3D movements of beads projected on the *xy*-plane (B) and the *xz*-plane (C). The movements of 8 randomly selected beads are indicated by the colored symbols. Bead trajectories are indicated by dotted lines. Scale bars = 10 μm.

during pseudopodial protrusion. In contrast, the values $\langle v'_{x\prime} \rangle$ at the front peripheral surface were positive with a relatively large standard deviation, which indicated that the beads on the front peripheral surface tended to move forward, although they highly fluctuated between the back and forward directions.

As shown in Fig. 3A and B, the y' components of the relative velocities, $v'_{x\prime}$, on the rear and central surfaces ($-1 < x'^{*} \leq 0$) were narrowly distributed around 0 μm/s. Together with the results for $v'_{x\prime}$, this indicated that the beads on the rear and central surfaces flowed linearly toward the rear peripheral surface. As shown in Fig. 3C, the speed of the organized flow was approximately 0.05 μm/s on the posterior half ($-1 < x'^{*} \leq -0.25$) of the cell surface. On the front cell surface ($0 < x'^{*} \leq 0.5$), the standard deviation of $\langle v'_{y\prime} \rangle$ in Fig. 3B was greater than that on the rear and central surfaces. Together with the results for $\langle v'_{x\prime} \rangle$ in Fig. 3B and $\langle |v'_{x\prime yz}| \rangle$ in Fig. 3C with larger standard deviations, this indicated that the beads on the front cell surface were rapidly and randomly fluctuating during leukocyte pseudopodial protrusion.

Regarding the *z*-direction, as shown in Fig. 3A and B, the relative velocity, v'_z, was 0 μm/s with a small standard deviation on each cell surface. This suggested that the bead movements were in-plane with the cell surface.

4. Discussion

In our experiments, fluorescent beads that were conjugated with Con A clearly showed heterogeneous physical behaviors be-

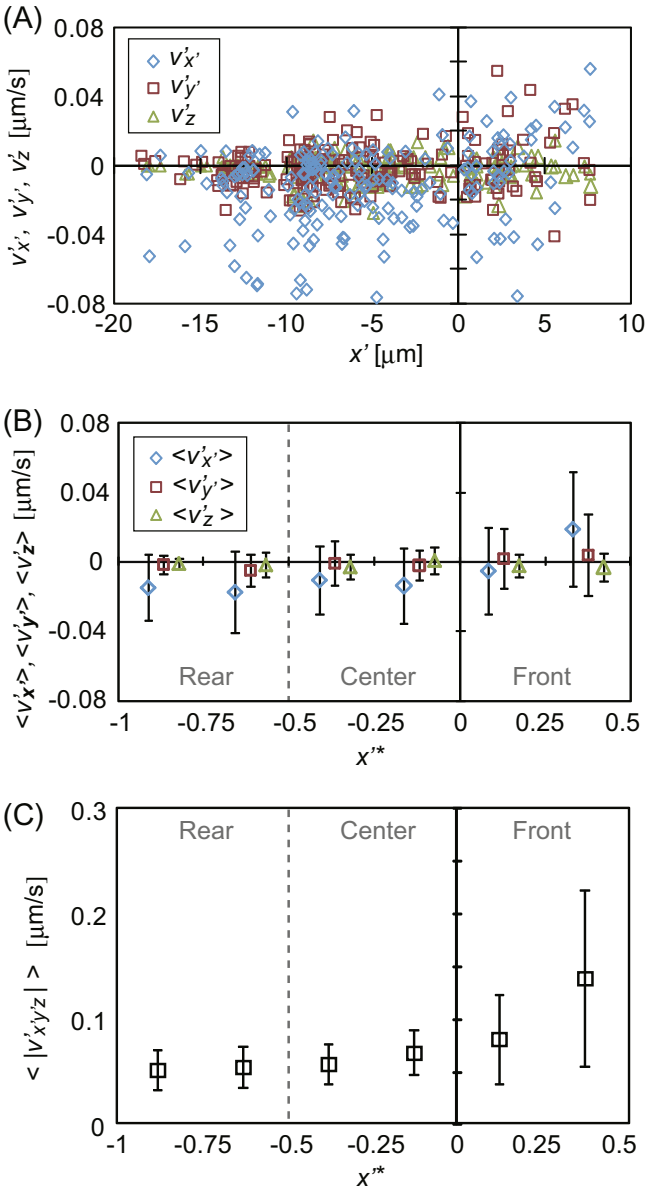

Fig. 3. Heterogeneity of bead movement dynamics on the rear, central, and front surfaces of leukocytes. (A) Relative velocities, $v'_{x'}$, $v'_{y'}$, and v'_z, are plotted against position x'. (B) Mean values, $\langle v'_{x'}\rangle$, $\langle v'_{y'}\rangle$ and $\langle v'_z\rangle$ of $v'_{x'}$, $v'_{y'}$, and v'_z, respectively, in (A) are plotted against x'^* (bin width: 0.25). (C) Mean values, $\langle |v'_{xyz}| \rangle$, of $|v'_{xyz}|$, are plotted against x'^* (bin width: 0.25). The rear, central, and front cell surfaces are defined as the regions with, $-1 < x'^* \leq -0.5$, $-0.5 < x'^* \leq 0$, and $0 < x'^* \leq 0.5$, respectively.

tween the rear, central, and front surfaces of leukocytes during pseudopodial protrusion. Beads that were initially on the rear and central dorsal surfaces of the cell body moved in directions opposite to that of the cell migration direction and converged to the rear peripheral surface. Simultaneously, the *z*-positions of these beads decreased because the cell body collapsed in the dorsal–ventral direction. In addition, it is noteworthy that those beads that moved into a newly formed pseudopodium exhibited rapid, random movements within the pseudopodium.

The organized flow of beads toward the rear peripheral surfaces of the leukocytes was presumably tightly coupled to the actin cortical flow in the backward direction. Similar cortical flow has been reported in migrating *Dictyostelium* cells [13,15], which are also known to exhibit pseudopodial amoeboid type movement. Based on our bead tracking data, the speed of the leukocyte cortical flow was estimated to be $|v'_{xyz}| = 0.05$ μm/s (Fig. 3C), which was of the same order as that reported for *Dictyostelium* cells of 0.05–0. 1 μm/s [13,15]. Cortical flow has long been recognized as a common basis for force generation in many animal cells for pulling cortical components, such as myosin, from regions of relaxation to those of contraction during cell migration and division [16,17]. Cortical flow is observed in cells that are detached from a substrate [13], which enables cell body deformation, even while in suspension. Therefore, cortical flow is assumed to critically contribute to flexible cell migration when loosely coupled to the ECM.

Interestingly, there were rapid, random bead movements on newly forming pseudopodial surfaces of leukocytes (Figs. 2B and C and 3B and C). This was clearly different from the organized retrograde flow of the actin meshwork that has been reported in protruding lamellipodia and lamella of fibroblasts [18,19], epithelial cells [20], and keratocytes [7–9]. These differences were hypothesized to have arisen from the differences in the interactions between the cell membrane and the actin cytoskeleton because the movement of a receptor on a viable cell surface is known to be affected by partial destruction of the actin cytoskeleton [14].

In our analysis, the diffusion coefficient for the beads on the surface of a newly forming pseudopodium was of the order of 1×10^{-10} cm^2/s. This was two to three orders of magnitude less than the diffusion coefficient of model trans membrane proteins incorporated into giant unilamellar vesicles, 1×10^{-9} to 1×10^{-8} cm^2/s [21,22]. In contrast, our estimate was an order of magnitude greater than the diffusion coefficient, 1×10^{-11} cm^2/s [14], of membrane receptors that strongly interacted with the actin cytoskeleton [23]. Thus, a comparison of these diffusion coefficients suggests that a newly forming pseudopodium of a leukocyte is characterized by actin cytoskeleton rupture and/or detachment of the plasma membrane from the actin cytoskeleton.

The significant collapse of the cell body in the dorsal–ventral direction along with the cortical flow that converged to the dorsal rear surface was assumed to play a role in expanding the cytoplasm into a newly forming pseudopodium. The mechanical properties of a deformable lipid membrane with less actin cytoskeletal back support in a newly forming pseudopodium facilitate cytoplasmic flow beyond a cortical defect. Fluid pressure-driven protrusion can occur in cells that are less adhesive to a substrate or even in cells while in suspension [24,25].

To the best of our knowledge, this is the first report to characterize the 3D modulation of cortical plasticity during pseudopodial protrusion by mouse leukocytes isolated from blood. Based on our results, leukocyte cortex physical behavior is characterized by cortical flow in the backward direction on the rear and central surfaces and by a cortical defect at the front surface that facilitates cytoplasmic flow. A leading edge protrusion caused by cytoplasmic flow can occur even in cells that are not adhering to a substrate. Although a frictional force between a cell and the ECM to hold the cell body is required for leukocytes to translocate, the magnitude of this frictional force is assumed to be significantly less than that required by mesenchymal cells. Indeed, two dimensional traction force microscopy revealed that the traction force exerted by migrating human leukocytes [26] was orders of magnitude less than that exerted by mesenchymal cells [27]. Furthermore, within *in vivo* and *in vitro* 3D environments, leukocytes can migrate without adhesion receptors by squeezing cytoplasm at the leading edge [24]. The 3D physical behavior of the leukocyte cortex characterized in this study would allow leukocytes to migrate while being minimally constrained by the ECM. Thus, this would be a fundamental property for flexible leukocyte migration to efficiently infiltrate and traverse almost any physiological environment.

Acknowledgments

We thank Yutaka Yamagata of the Ultrahigh Precision Optics Technology Team, RIKEN Center for Advanced Photonics, for helpful discussions. We thank the Support Unit for Animal Resources Development at the RIKEN Brain Science Institute for help with primary cell cultures. This work was partially supported by "Cell-type specific design concept of functional microstructured surfaces for non-invasive cell sorting", Adaptable and Seamless Technology Transfer Program through Target-driven R&D, JST, and Grant-in-Aid for Scientific Research (25630046), JSPS.

References

[1] J. Renkawitz, M. Sixt, Mechanisms of force generation and force transmission during interstitial leukocyte migration, EMBO Rep. 11 (2010) 744–750.
[2] P. Friedl, K. Wolf, Plasticity of cell migration: a multiscale tuning model, J. Cell Biol. 188 (2010) 11–19.
[3] T. Lammermann, M. Sixt, Mechanical modes of 'amoeboid' cell migration, Curr. Opin. Cell Biol. 21 (2009) 636–644.
[4] E. Paluch, C. Sykes, J. Prost, M. Bornens, Dynamic modes of the cortical actomyosin gel during cell locomotion and division, Trends Cell Biol. 16 (2006) 5–10.
[5] H. Miyoshi, J.M. Ju, S.M. Lee, D.J. Cho, J.S. Ko, Y. Yamagata, T. Adachi, Control of highly migratory cells by microstructured surface based on transient change in cell behavior, Biomaterials 31 (2010) 8539–8545.
[6] K. Rottner, T.E.B. Stradal, Actin dynamics and turnover in cell motility, Curr. Opin. Cell Biol. 23 (2011) 569–578.
[7] T. Adachi, K.O. Okeyo, Y. Shitagawa, M. Hojo, Strain field in actin filament network in lamellipodia of migrating cells: implication for network reorganization, J. Biomech. 42 (2009) 297–302.
[8] C. Jurado, J.R. Haserick, J. Lee, Slipping or gripping? fluorescent speckle microscopy in fish keratocytes reveals two different mechanisms for generating a retrograde flow of actin, Mol. Biol. Cell 16 (2005) 507–518.
[9] M.F. Fournier, R. Sauser, D. Ambrosi, J.J. Meister, A.B. Verkhovsky, Force transmission in migrating cells, J. Cell Biol. 188 (2010) 287–297.
[10] P. Vallotton, S.L. Gupton, C.M. Waterman-Storer, G. Danuser, Simultaneous mapping of filamentous actin flow and turnover in migrating cells by quantitative fluorescent speckle microscopy, Proc. Natl. Acad. Sci. USA 101 (2004) 9660–9665.
[11] P. Vallotton, J.V. Small, Shifting views on the leading role of the lamellipodium in cell migration: speckle tracking revisited, J. Cell Sci. 122 (2009) 1955–1958.
[12] Y.L. Wang, J.D. Silverman, L.G. Cao, Single particle tracking of surface receptor movement during cell division, J. Cell Biol. 127 (1994) 963–971.
[13] S. Yumura, G. Itoh, Y. Kikuta, T. Kikuchi, T. Kitanishi-Yumura, M. Tsujioka, Cell-scale dynamic recycling and cortical flow of the actin–myosin cytoskeleton for rapid cell migration, Open Biol. 2 (2013) 200–209.
[14] Y. Sako, A. Kusumi, Compartmentalized structure of the plasma membrane for receptor movements as revealed by a nanometer level motion analysis, J. Cell Biol. 125 (1994) 1251–1264.
[15] P.Y. Jay, E.L. Elson, Surface particle transport mechanism independent of myosin II in dictyostelium, Nature 356 (1992) 438–440.
[16] D. Bray, J.G. White, Cortical flow in animal-cells, Science 239 (1988) 883–888.
[17] R.L. DeBiasio, G.M. LaRocca, P.L. Post, D.L. Taylor, Myosin II transport, organization, and phosphorylation: evidence for cortical flow/isolation–contraction coupling during cytokinesis and cell locomotion, Mol. Biol. Cell 7 (1996) 1259–1282.
[18] A. Harris, G. Dunn, Centripetal transport of attached particles on both surfaces of moving fibroblasts, Exp. Cell Res. 73 (1972) 519–523.
[19] M. Abercrombie, J.E. Heaysman, S.M. Pegrum, The locomotion of fibroblasts in culture: III. Movements of particles on the dorsal surface of the leading lamella, Exp. Cell Res. 62 (1970) 389–398.
[20] C.M. Waterman-Storer, A. Desai, J.C. Bulinski, E.D. Salmon, Fluorescent speckle microscopy, a method to visualize the dynamics of protein assemblies in living cells, Curr. Biol. 8 (1998) 1227–1230.
[21] M.K. Doeven, J.H.A. Folgering, V. Krasnikov, E.R. Geertsma, G. van den Bogaart, B. Poolman, Distribution, lateral mobility and function of membrane proteins incorporated into giant unilamellar vesicles, Biophys. J. 88 (2005) 1134–1142.
[22] Y. Gambin, R. Lopez-Esparza, M. Reffay, E. Sierecki, N.S. Gov, M. Genest, R.S. Hodges, W. Urbach, Lateral mobility of proteins in liquid membranes revisited, Proc. Natl. Acad. Sci. USA 103 (2006) 2098–2102.
[23] N. Morone, T. Fujiwara, K. Murase, R.S. Kasai, H. Ike, S. Yuasa, J. Usukura, A. Kusumi, Three-dimensional reconstruction of the membrane skeleton at the plasma membrane interface by electron tomography, J. Cell Biol. 174 (2006) 851–862.
[24] T. Lammermann, B.L. Bader, S.J. Monkley, T. Worbs, R. Wedlich-Soldner, K. Hirsch, M. Keller, R. Forster, D.R. Critchley, R. Fassler, M. Sixt, Rapid leukocyte migration by integrin-independent flowing and squeezing, Nature 453 (2008) 51–55.
[25] G. Charras, E. Paluch, Blebs lead the way: how to migrate without lamellipodia, Nat. Rev. Mol. Cell Biol. 9 (2008) 730–736.
[26] L.A. Smith, H. Aranda-Espinoza, J.B. Haun, M. Dembo, D.A. Hammer, Neutrophil traction stresses are concentrated in the uropod during migration, Biophys. J. 92 (2007) 58–60.
[27] S. Munevar, Y.L. Wang, M. Dembo, Traction force microscopy of migrating normal and H-ras transformed 3T3 fibroblasts, Biophys. J. 80 (2001) 1744–1757.